Identification and Inversion of Magnetic Hysteresis for Sinusoidal Magnetization

Martin Kozek, Bernhard Gross

Vienna University of Technology
Institute of Mechanics and Mechatronics
Division of Control and Process-Automation
A-1040 Vienna, Austria

Abstract— **The sinusoidal magnetization of a sample material is difficult to achieve, since the magnetic hysteresis poses a strong non-linearity. In order to find the proper input voltage, a feed-forward strategy with a hysteresis model identification and inversion is proposed. The classical Preisach model in the Everett formulation is used for this purpose and eddy current effects are also included. A new heuristic inversion offering equal performance but avoiding a time-consuming identification procedure is also proposed. After an initial identification procedure the model, its inverse, the heuristic inversion, and the proper input voltages for a desired sinusoidal magnetization are computed. The resulting application achieves accurate results, is easy to use, supplies the user with transparent and clear information, and adds the flexibility for automation or remote control.**

Keywords— **magnetic hysteresis, model inversion, virtual instrumentation**

I. Introduction

The experimental setup described in ASTM A 932/A 932M-95 [1] for measuring the magnetic characteristics of steel sheet samples is used for recording the magnetic hysteresis of the sample material. The magnetization of the material should be an undistorted sine-function with frequencies ranging from 10 to 500 Hz. In the original standard only analogue gauges are mentioned, however, both the execution of the experiment as well as the de-magnetization of the sample and the processing of measured data are achieved by virtual instrumentation.

The instruction for a sinusoidal magnetization is demanding since the magnetic hysteresis of a material requires a non-sinusoidal input voltage. Therefore, the sine-shape could be guaranteed using both feed-forward and feed-back control. This paper is focused on the realization of the feed-forward part of a control scheme. In order to demonstrate the feasibility of this concept, a model inversion of a combined electric and magnetic hysteresis model is utilized. Using a laptop-computer with LabVIEW and MATLAB the parameters of the hysteresis model are automatically identified and the necessary magnetic field and the input voltage are computed accordingly.

The physical foundations of magnetic materials are relatively well understood, and a detailed description can be found elsewhere (e.g. [4]). The choice of a proper hysteresis model for a given purpose is critical for the present problem, and good overview over different model types can be found in [17]. In the present application the classical Preisach model in the Everett formulation, as described in [8], was used. The main advantages are a comparatively simple implementation of the identification and inversion procedure, which is also the reason why this type of model has been frequently used for the compensation of hysteresis phenomena in actuators ([14], [15], [19], [20]). An extensive presentation of the Preisach model can be found in [7], and the identification methods are described in [10]. The heuristic inversion proposed in this paper is not based on an explicit model of the hysteresis, and therefore, it does not require an identification procedure with extensive measurements. Instead, only a comparatively short experiment is necessary for the computation of the appropriate input voltage.

The paper is structured as follows: In section II a short introduction to the principles and nomenclature of magnetic hysteresis is given and the mathematical model is derived. The identification and inversion principle is outlined. The implementation of the inversion together with a new inversion method is described in more detail in section III. The following section IV describes the experimental setup and the hardware used in the experiments. In section V the software tools and their interaction as well as the user interface are presented. The performance of the implemented algorithms along with results from experiments are explained in section VI. A short roundup of the main ideas concludes the paper.

II. Magnetic Hysteresis

A. Fundamentals

When a magnetic field – e.g. of a current carrying coil – acts on a material, both permanent and induced magnetic dipoles are oriented accordingly. This property is quantified by means of the magnetization M. The resulting magnetic induction is comprised of the part from the coil $\mu_0 H$ and of the part from the material $\mu_0 M$, which is also called polarization J:

$$B = \mu_0 (H + M) . \tag{1}$$

The relation $B(H)$ is shown schematically in fig. 1. The magnetic induction increases according to the

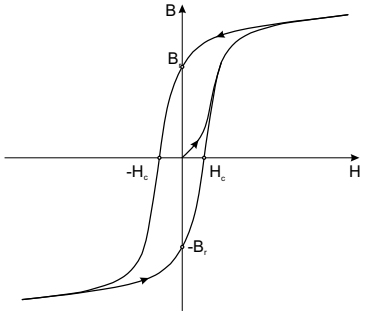

Fig. 1. Major hysteresis loop

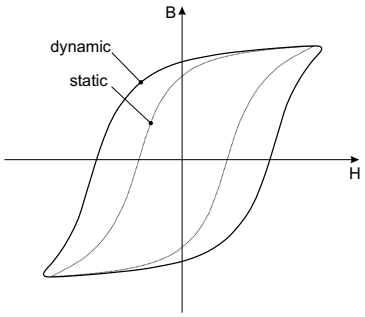

Fig. 2. Dynamic versus static loop

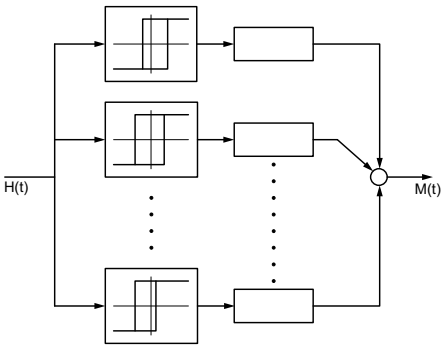

Fig. 3. Preisach model

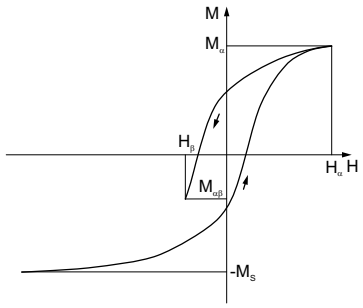

Fig. 4. FOD curve

outer magnetic field H, caused by a growing number of oriented dipoles. Due to saturation a maximum magnetization M_S exists, which is the so-called saturation-magnetization. The total field can now only increase by the outer field from the coil (linear parts of the curve). A reduction of the magnetic field leaves a remainder of magnetization even when the outer field intensity is zero. This remanence B_r is the starting point for an inversion in the magnetic field. Only when the converse field has an intensity of H_c (coercive intensity) the overall magnetic induction is zero. For growing negative values of the outer field saturation occurs as before.

This non-linear static relation between B and H including the past progression of the flux density is called the magnetic hysteresis. A very important dynamic effect is the expansion of the hysteric curve at higher frequencies due to eddy currents (see fig.2).

B. Model

The model inversion demands several properties of a hysteresis model:

- Simple and fast computation of flux density B and magnetization M, respectively.
- A wide range of materials where the model is valid (both magnetic hard and soft).
- Simple and robust identification of model parameters.
- The model must be invertible.

The Preisach model complies with all these demands in a harmonic way and is therefore chosen as proper model structure.

B.1 Classical Preisach Model (CPM)

The CPM defines the hysteresis loops by a parallel connection of individual hysterons (see fig.3). The hysterons are simple 2-state relays with hysteresis, where the upper switching point is α_i, the lower switching point is β_i, and the output is defined by

$$\phi(t) = \begin{cases} -1 & : \quad H(t) \leq \beta \\ +1 & : \quad H(t) \geq \alpha \\ \pm 1 & : \quad \beta < H(t) < \alpha \end{cases} \tag{2}$$

Only hysterons with $\alpha \geq \beta$ are physically meaningful, due to their energy dissipating property. In the case $\alpha = \beta$ the hysterons may switch reversibel. The set of all possible hysterons P is defined by:

$$P = \left\{ (\alpha, \beta) \in I\!R^2 \, | \alpha \geq \beta \right\}. \tag{3}$$

Without further details it is noted that the efficient computation is achieved by means of the Everett integral or Everett function

$$E\left(H_\alpha, H_\beta\right) = M_\alpha - M_{\alpha\beta}, \tag{4}$$

which can be found by measuring the so-called First-Order-Descending (FOD) curves (see fig.4). The resulting hysteresis is then described by

$$\begin{aligned} M\left(H\left(t\right)\right) = -M_S \quad &+ \quad \sum_{i=1}^{k-1} E\left(H_{d,i+1}, H_{d,i}\right) \\ &+ \quad E\left(H\left(t\right), H_{d,k}\right). \end{aligned} \tag{5}$$

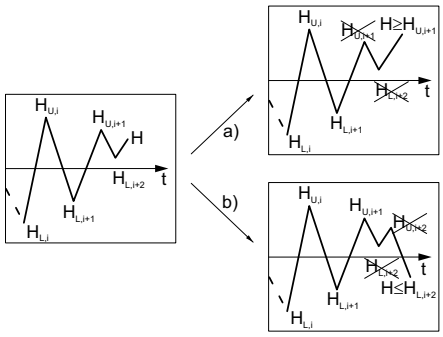

Fig. 5. Wiping out property

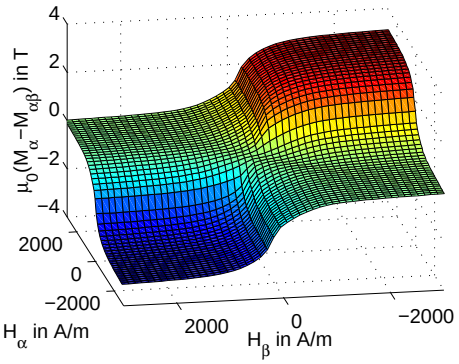

Fig. 6. Example of an Everett map. For better readability H_β is plotted in reverse direction.

The $H_{d,i}$ define the dominant extremes

$$\begin{aligned} H_d &= \{H_{d,i}\} = \{H_{L,1} = \\ &= -H_S, H_{U,1}, H_{L,2}, H_{U,2}, H_{L,3}, \dots \\ &\quad \dots H_{U,m} \text{ or } H_{L,n}\}, \end{aligned} \tag{6}$$

which are subsets of all previous maxima

$$\begin{aligned} H_U(t) &= \{H_{U,1}(t_{U,1}), H_{U,2}(t_{U,2}), \dots \\ &\quad \dots H_{U,m}(t_{U,m})\}, \end{aligned} \tag{7}$$

and minima

$$\begin{aligned} H_L(t) &= \{H_{L,1}(t_{L,1}), H_{L,2}(t_{L,2}), \dots \\ &\quad \dots H_{U,n}(t_{L,n})\}. \end{aligned} \tag{8}$$

These subsets are ordered both in time $t_{L,1} < t_{U,1} < t_{L,2} < t_{U,2} < \dots < t$ as well as in magnitude $H_{L,1} < H_{L,2} < \dots < H_{L,n} < H(t)$ and $H_{U,1} > H_{U,2} > \dots > H_{U,m} > H(t)$, respectively. If the current magnetic field is greater than a stored lokal maximum (fig.5,a), the stored maximum and all consecutive maxima and minima are wiped out. If the magnetic field is smaller than a stored minimum the situation is completely analogous (fig.5,b). This characteristic of the Preisach model is called the wiping out property and facilitates an efficient description of the magnetic state.

B.2 Extensions to the CPM

The CPM is a description of hysteresis which is in many ways idealized. Especially the congruency of small loops and the wiping-out property are not fulfilled by many hysteretic phenomenons. Therefore, numerous static extensions have been proposed (see e.g. [6], [7] for a survey) which provide additional functionality in order to model more complex features.

Another important extension is the coverage of dynamic phenomena, mainly eddy current effects. They are either modeled by modified hysterons [3], an additional magnetic state [9], rate-dependend Preisach functions [18], [2], and Hammerstein structures [13]. All of these extension are useful in approximating a given hysteresis function, however, the inversion of these extended models is either impossible or extremely complex.

B.3 Coleman-Hodgdon Model

An alternative formulation for hysteresis is given by the Coleman-Hodgdon model (CHM) ([5], [11], [12]). In contrast to the CPM it consists of a differential equation, where the history is not any longer implicitely stored, but it has to be added through the initial conditions:

$$\dot{H} = \alpha|\dot{B}|\,[f(B) - H] + \dot{B}g(B) \tag{9}$$

The functions $f(B)$ and $g(B)$ are specific to a material and most model parameters may be reconstructed from a measured hysteresis loop, only one parameter has to be adapted iteratively. Similar to the CPM there exist also dynamic extensions to the CHM.

The CHM is very easy to implement and therefore well suited for simulation purposes.

B.4 Identification

The identification of the CPM is accomplished by measuring multiple FOD curves which in turn defines the Everett map. For the measurements it is important to note that $H_\alpha \geq H_\beta$ holds (see fig.4) and therefore only one half of the Everett map may be constructed by measurements. The remaining values may be completed using

$$E(H_\alpha, H_\beta) = -E(H_\beta, H_\alpha) \;\forall\, H_\alpha < H_\beta. \tag{10}$$

The Everett map $E(H_\alpha, H_\beta)$ may therefore be computed from a double integral over a triangular set P_E:

$$E(H_\alpha, H_\beta) = 2 \iint_{P_E} \mu(\alpha, \beta)\, d\alpha\, d\beta. \tag{11}$$

It is the so-called Everett integral and constitutes the Everett map; an example is depicted in fig.6. Performing a double partial differentiation with respect to H_α and H_β yields the value of the Preisach function at the coordinates $(H_\alpha = \alpha, H_\beta = \beta) \in P_E$:

$$\mu(H_\alpha, H_\beta) = -\frac{1}{2} \frac{\partial^2 E(H_\alpha, H_\beta)}{\partial H_\alpha\, \partial H_\beta} \tag{12}$$

By measuring several FOD-curves the Everett map $E(\alpha, \beta)$ may be constructed in a point-wise fashion, and consequently, the Preisach function may be computed using the relation 12.

It should be emphasized that a double differentiation of measured data as required by 12 is very problematic. The applicability of this approach critically depends on the quality of the measured data, which in turn is closely coupled to both hardware specifications and measurement procedures. Obviously, an alternative formulation without any differentiation would be preferable since it completely avoids the inherent problems of noise amplification.

A straightforward approach to achieve this goal is using (5), where the magnetization is directly computed from the dominant extremes $H_{d,i}$. Reformulating this equation utilizing the already computed values $M_{d,k}$ a simple equation results:

$$M(H(t)) = M_{d,k} + E(H(t), H_{d,k}). \tag{13}$$

Only Everett integrals have to be evaluated in (13), and they may be directly computed from measured FOD-curves. Hence, the computation of the current magnetization requires only storage of the dominant extremes, computation of the Everett integrals, and interpolation between measured values in order to establish a dense grid on the Everett map.

B.5 Inversion

The Inversion of the CPM is carried out by computing the inverse of the Everett map F, defined by

$$F(M_\alpha, M_{\alpha\beta}) = H_\alpha - H_\beta. \tag{14}$$

the unknown magnetic field may be computed by [20]

$$\begin{aligned} H(M(t)) &= -H_S + \sum_{i=1}^{k-1} F(M_{d,i+1}, M_{d,i}) \\ &\quad + F(M(t), M_{d,k}) \\ &= H_{d,k} + F(M(t), M_{d,k}). \end{aligned} \tag{15}$$

$F(M_\alpha, M_{\alpha\beta})$ may be computed from $E(H_\alpha, H_\beta)$. For given values of M_α and $M_{\alpha\beta}$ the following approach is pursued: For the ascending branch of the FOD curve the relation

$$M_\alpha = -M_S + E(H_\alpha, -H_S) \tag{16}$$

holds, and the respective H_α may be computed by interpolation. The missing value of H_β can finally be retrieved by utilizing the definition of the Everett map

$$E(H_\alpha, H_\beta) = M_\alpha - M_{\alpha\beta},$$

using the value from (16) of H_α. Now, the difference between $H_\alpha - H_\beta$ in (14) may be computed and the Everett function of the inverse model is constituted. The computation is carried out similar to section II-B.1, only H and M are interchanged.

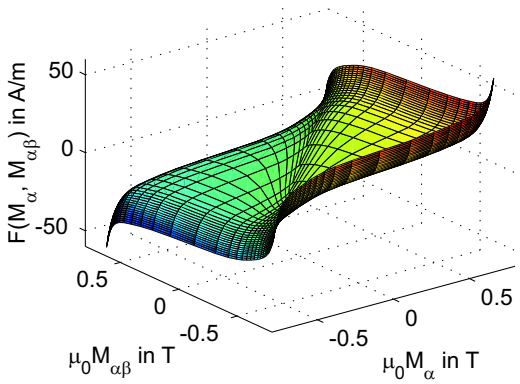

Fig. 7. Inverse Everett map

III. Implementation of Inversion

A. Inverse Everett Map

Using the method described in section II-B.5, the Everett map is constructed using FOD curves. The inverse Everett map is then computed utilizing (14). A typical inverse Everett map is depicted in fig.7. Note that the original regular grid (as plotted in fig.6) is strongly distorted due to the non-linear nature of the inversion. The grid spacing is closely related to the accuracy of the inversion. Especially for a small magnetization a fine grid will show a better performance. In order to achieve a small meshed grid additional points are interpolated.

The model inversion using the Everett map is also numerically efficient. A map spanned by a 100x100 grid is inverted within seconds using Matlab running on a standard personal computer.

B. Heuristic Inversion

A new heuristic approach was also developed and implemented. This method utilizes the periodic nature of the desired magnetization and the facts that the relationship between Magnetization and the intensity of the magnetic field is purely static in the Preisach model, and that they depend on the dominant extremes. In order to compute an estimate of the necessary magnetic field $\hat{H}_{CP}$ for a desired magnetization $J_S(t)$, the time-difference between the measured relationship $J_M(H_M)$ and the desired trajectory may be used as a correcting factor. The only necessary condition for this approach is a periodic trajectory and a monotonuous FOD curve.

In fig.8 a schematic drawing for a sinusoidal magnetization is shown. The proposed approach corresponds to a simultaneous distortion of the time-axis of the measured data $H(t)$ and $J(t)$. Care must be taken that the desired maximum magnetization is accurately met during the data acquisition, otherwise large deviations due to the non-linearity may result. The desired sinusoidal magnetization is given by

$$J_S = A_S \cos(2\pi f t) \tag{17}$$

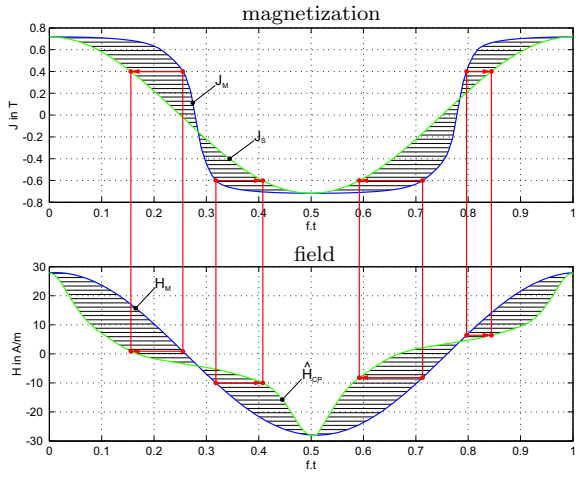

Fig. 8. Heuristic inversion of periodic signal

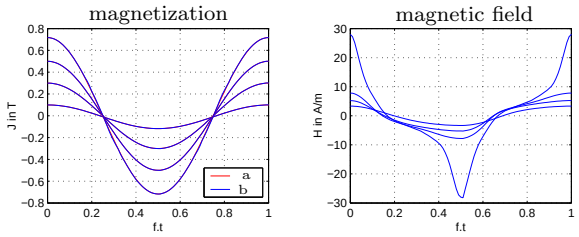

Fig. 9. Simulation results for heuristic inversion

and the corrected time-axis between measured and necessary magnetic field is then given by

$$t_i = \begin{cases} \dfrac{1}{2\pi f}\cos^{-1}\left(\dfrac{J_M(t)}{A_S}\right), 0 \le ft \le \dfrac{1}{2} \\ \dfrac{1}{2\pi f}\left[2\pi - \cos^{-1}\left(\dfrac{J_M(t)}{A_S}\right)\right], \dfrac{1}{2} < ft \le 1 \end{cases} \tag{18}$$

The necessary magnetic field can be written in compact form as

$$\hat{H}_{CP}(t_i) = H_M(t). \tag{19}$$

For equi-distant sampling instants (as requiered by digital signal processing) an interpolation can be performed (e.g. using cubic splines).

In fig.9 simulation results of the heuristic method applied to a Preisach model are shown. The actual (b - blue) and the desired (a - red) magnetization are almost identical if the maximum magnetization is accurately met. Consequently, the proposed method is very well suited for the given problem of guaranteeing a sinusoidal magnetization. The main advantage lies in the fact that no time-consuming identification of a hysteresis model is necessary, and the computational expense is also very low. The need for accurately achieving the desired maximum magnetization, however, poses a clear restricition on the measuring procedure.

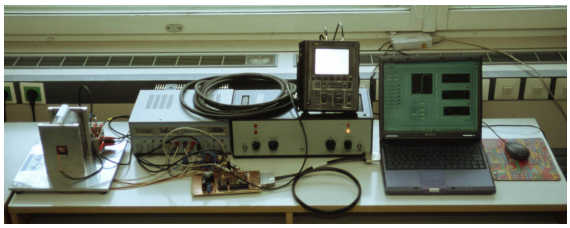

Fig. 10. Fotograph of the experimental setup

C. Computation of Input Voltage

Based on the desired magnetization M and the appropriate magnetic field H_{CP}, which has been computed using the inverse hysteresis model, the magnetic induction results as

$$B = \mu_0 \left(H_{CP} + M\right). \tag{20}$$

In order to account for the approximate effect of eddy currents the actual necessary magnetic field becomes

$$H = H_{CP} + \frac{\sigma d^2}{12}\frac{dB}{dt}, \tag{21}$$

where d is the thickness of the sample and σ is the inverse resistance. The current in the primary circuit can be computed using the length of the magnetic path l_M, the number of windings of the primary coil of the yoke N_{Yp}, and the necessary magnetic field:

$$i = \frac{l_M}{N_{Yp}}H. \tag{22}$$

The necessary input voltage u_I can now be calculated, using the cross section of the sample A_S, the ohmic resistance of the primary yoke coil R_{Yp}, the measuring resistor R_H, and the mutual inductor R_{MI}, respectively, and the inductance L_{MI}:

$$u_I = \frac{1}{A_P}\left[N_{Yp}A_S\frac{dB}{dt} + \left(R_{Yp} + R_H + R_{MI}\right)i + L_{MI}\frac{di}{dt}\right] \tag{23}$$

IV. EXPERIMENTAL SETUP

The experimental setup depicted in fig.10 consists of the following components: lap-top computer & software, multifunction I/O card, control board PCB1, signal-conditioning board PCB2, power amplifier, and plant. Data acquisition and control of the experimental setup was realized using the software LabVIEW 6.0. The tasks of data acquisition and post-processing were split up between LabVIEW and MATLAB. LabVIEW clearly has advantages concerning speed of data acquisition and flexibility of measuring procedure, however, the effort and complexity of programming is minimized using MATLAB. The schematic interaction between the components can be seen in fig.11. A DAQCard-6062E from National Instruments

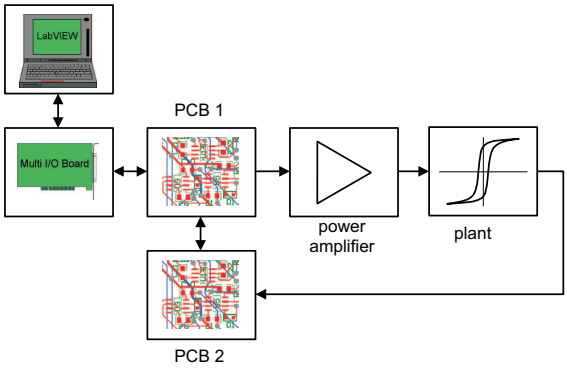

Fig. 11. Block-diagram of the experimental setup

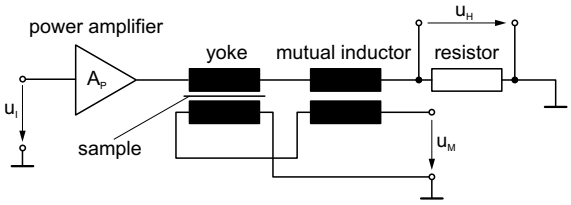

Fig. 12. Block diagram of plant

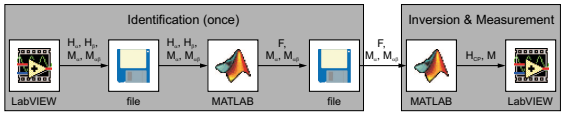

Fig. 13. LabVIEW-MATLAB interaction

with a maximum sampling rate of $(500 kS/s)$ was used as data acquisition hardware and also for control input and output. The two analogue outputs feature update rates of up to $(850 kS/s)$. Additionally, 8 digital TTL/CMOS compatible inputs/outputs are available, which were used for the control of the connected custom made control boards PCB1 and PCB2.

A. Control Boards PCB1 and PCB2

PCB1 acts as an interface between measuring device and the experimental setup. On board are two anti-aliasing filters which can be tuned using 8 bit for each filter, and several analogue switches for different control tasks. The 8 digital inputs and outputs of the board are used as outputs only. They tune the bandwidth and gain of the filters, control the analogue switches, which govern the signal routing, and the remaining output is dedicated to reset the integrator on board of PCB2.

Board PCB2 is only built for signal conditioning purposes. It has 2 channels with the possibility of AC or DC coupling, respectively. Both channels allow for the measurement of signals with voltage ranges as high as $\pm 50\, V$. For protection of the filters an additional voltage limitation is implemented. Channel 1 features the additional possibility of integrating the measured input.

B. Power Amplifier

An appropriate power amplifier must provide DC capabilities in order to guarantee proper measuring of the FOD curves. Minimum drift and offset are also prerequisite.

C. Plant

The plant consists of a magnetic yoke (layered iron sheets), a mutual inductor (compensation of magnetic air flux), and a measuring resistor. The block-diagram is depicted in fig.12. The physical units of the measured variables can be computed by

$$M(t) = \frac{1}{\mu_0 N_{Ys} A_S} \int u_M(t) dt \qquad (24)$$

and

$$H(t) = \frac{N_{Yp}}{l_M R_H} u_H(t). \qquad (25)$$

from the measured voltages u_M and u_H. N_{Yp} and N_{Ys} are the primary and secondary number of windings of the yoke, A_S is the cross-section of the sample, l_M is the length of the magnetic path inside the sample, R_H is the resistance of the measuring resistor, and μ_0 is the magnetic field constant.

V. Software

The software necessary for controlling the experiments essentially comprises two virtual instruments: *identES.VI* for measuring the FOD curves, and *PreiSin.VI* for the feed-forward control of the experiment. The interaction between MATLAB and LabVIEW and the course of an experiment is depicted in fig.13.

The identification of the hysteresis model is done as described in section II-B.4 by measuring several FOD curves and consists of two steps. In the first step the Everett map is constructed using *identES.VI*, and in the second step the inverse of this map is computed.

The user-interface of the above described identification-VI (fig.14) is structured into 3 alternative windows. The functionality comprises input of setup-data, choice of de-magnetization procedure, and identification parameters. Measured raw voltage and the result of the averaging process is plotted on-line as a quick check-up.

After the identification has been started the FOD curves are measured. Once an individual FOD curve has been recorded, an average over all periods is computed and the necessary values H_α, H_β, M_α, and $M_{\alpha\beta}$ are extracted and stored in matrices.

The second step is the computation of the inverse Everett map $F(M_\alpha, M_{\alpha\beta})$, which is performed completely outside of LabVIEW using MATLABs computational power in vector/matrix calculations.

The control of the experimental setup is done by the Virtual Instrument *PreiSin.VI* (fig.15). The desired amplitude and frequency of the sine-function can be

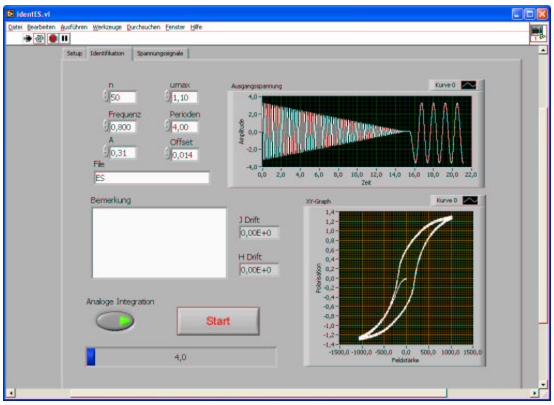

Fig. 14. Identification GUI 'identES.VI'

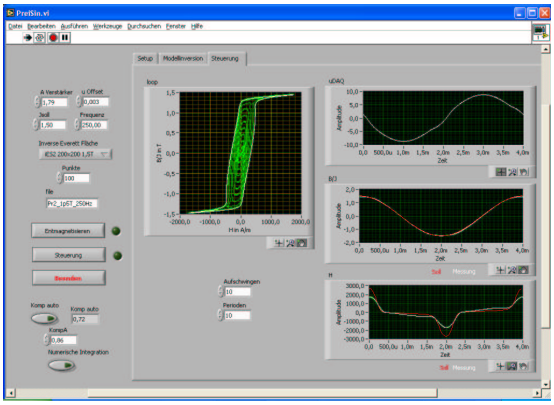

Fig. 15. Experimental GUI 'PreiSin.VI'

chosen deliberately by the user.

Before the feed-forward experiment is started, the according inverse Everett map is loaded inside a MATLAB node, and the theoretically correct static magnetic field H_{CP} is computed considering the desired amplitude. Finally, the necessary input voltage to the plant u_I is computed as specified in section III-C, and this voltage is fed into the power amplifier.

VI. Results

Using the software described in section V the performance of an experiment is straightforward and efficient. A laptop-computer with measurement-hardware is sufficient, no other measuring devices are needed. All signals and important physical quantities can be displayed or accessed easily.

A. Preisach Model Validation

The Preisach model is validated against measured data, since it is used for simulation of all the proposed methods. Especially for the inversion a structural correct and accurate model is pre-requisite for a satisfactory result.

In fig.16 the measured (a - red) and simulated (b - blue) hysteresis loop for a stell specimen is plotted. The shape and values of the major loop are very accurate, only the inner loops show deviations around

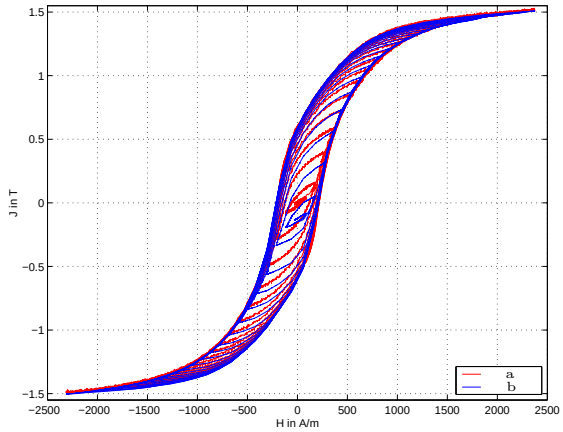

Fig. 16. Comparison of measured and simulated hysteretic loops. Simulation from 50x50 grid.

the origin. The plotted results were computed from a 50x50 grid for the Everett map, additional runs with 200x200 grids yielded better results at the cost of an extended time-span for identification. Closer investigations of the sensitivity of the system with respect to measurement offsets revealed a very strong influence of small systematic errors. In particular the amplifier has to meet very high standards in order to achieve good agreement between measurement and simulation. The mathematical model, however, is very accurate.

B. Inversion - Everett Map

The inversion of the Preisach model utilizing the inverse Everett map has been described in detail earlier (section II-B.5). Nevertheless, there are two ways to compute the inverse Everett map:

- Direct identification of the inverse Everett map from measured data.
- Identification of the Everett map and subsequent computation of the inverse.

Both methods have been implemented and validated against measurements.

In fig.17 three different results for the inverse Everett map are plotted. On top the directly identified map from measured data is plotted. Due to poor repeatability of the measurements (possible reasons are drifts in the integrator and the amplifier) a rough surface results. It is clearly not suitable for the computation of the magnetization.

The middle plot is the result for the identification of the Everett map and its inversion. A much smoother surface results, only the right border is jagged due to measurment noise. Exploiting the symmetry $J_{\alpha\beta} = -J_{\alpha}$ of the inverse map, the smooth left side is mirrored onto the right area. Using this procedure the bottom plot with an overall smooth and accurate inverse Everett map results. In the remainder of this section this map is used for computation of the necessary magnetic field.

In fig.18 the most important signals for 2 magnetic polarizations (1.5 and 1 Tesla) at 4 different frequencies (1, 10, 100, and 225 Hertz) are plotted. The x-axis

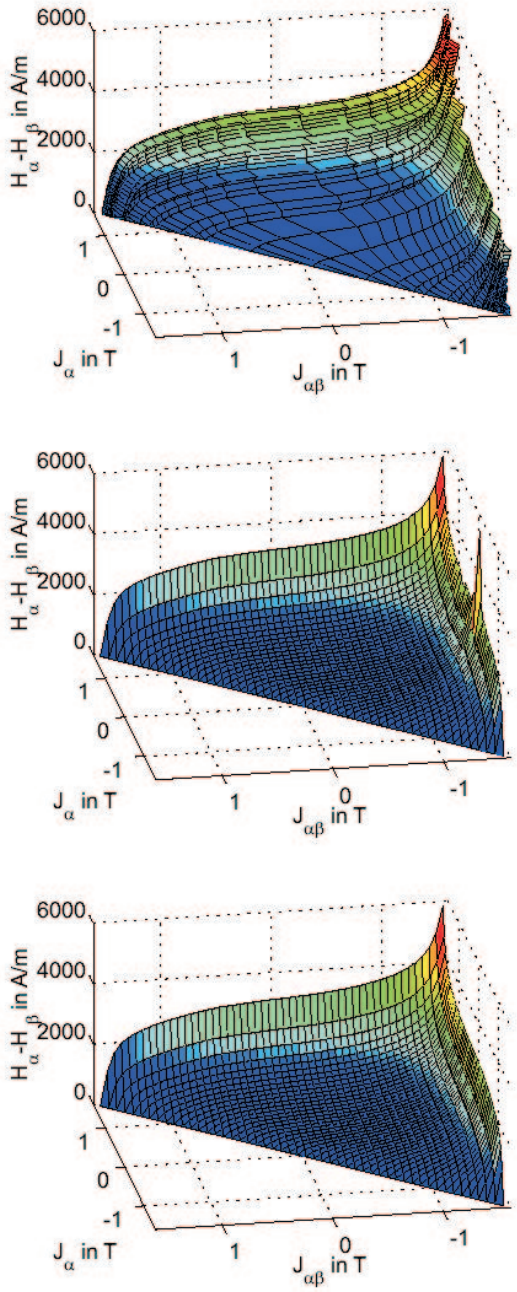

Fig. 17. Inverse Everett map. top: direct measurement, middle: inversion from measured Everett map, bottom: inversion using mirroring

of each plot is scaled over one period regardless of the frequency. In the first row, the magnetic polarization is depicted. The desired signal is a undistorted sine-function (red line) and the measured polarization is in good agreement, especially for small to medium polarizations. With higher levels of polarization, model deviations have a stronger impact and slight distortions cannot be avoided. The magnetic field depicted in the

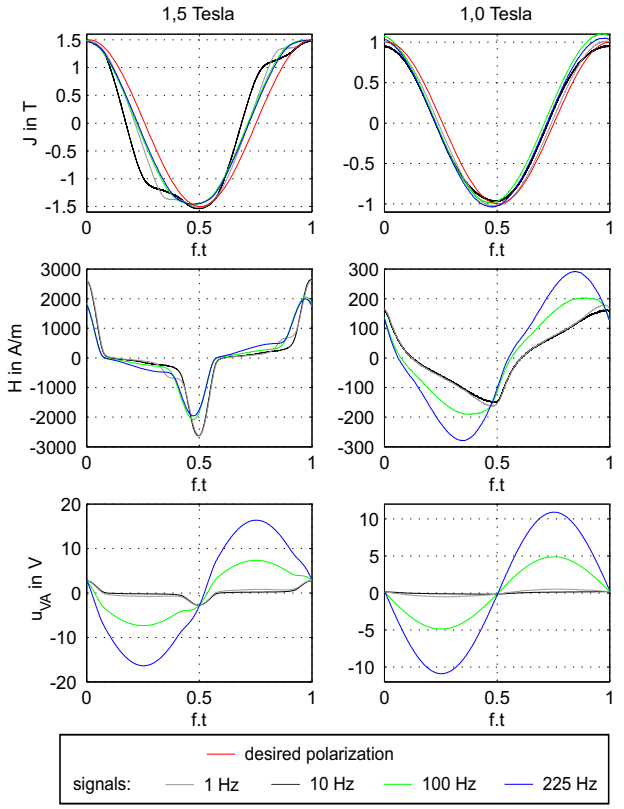

Fig. 18. Experimental results for inversion of Everett map. Left column: maximum polarization of 1.5 Tesla, right column: maximum polarization of 1 Tesla. Top row: magnetic polarization, second row: magnetic field, third row: input voltage.

second row clearly shows a strong non-linear behavior which is directly correlated to the hysteresis loop. The dependence on frequency is mainly caused by eddy currents, however, the implemented model for these dynamic effects does also contribute to the distortions visible in the magnetic polarization. The third row shows the measured input voltage which is close to a pure sine-function for high frequencies, regardless of the polarization. This effect can be explained by (23) where the part $\frac{dB}{dt}$ becomes dominant for higher frequencies. For low frequencies the non-linear behavior of the experimental setup is clearly visible in the input voltage.

Apparently, using only feed-forward control the main non-linearities of the experimental setup were already removed for a wide variety of frequencies and polarizations and whatever distortions remain in the polarization could be compensated by means of an additional feed-back controller.

C. Inversion - Heuristic Method

When implementing the heuristic method great care must be taken in order to guarantee that the maximum desired magnetization is actually met. This can be achieved manually with arguable effort, it could also be done by an automated procedure provided that

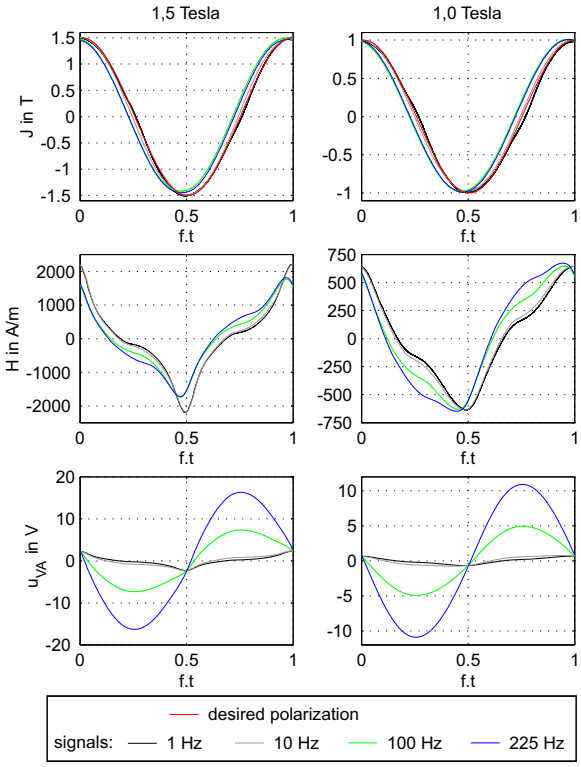

Fig. 19. Experimental results for heuristic inversion. Left column: maximum polarization of 1.5 Tesla, right column: maximum polarization of 1 Tesla. Top row: magnetic polarization, second row: magnetic field, third row: input voltage.

the drifts in the measuring chain can be minimized.

Using the method presented in section III-B and applying it to the same setup as described in the section above, the results plotted in fig.19 are achieved. Apparently, the heuristic method yields the same or even better results with much less computational effort. This result clearly justifies the recommendation to implement the heuristic method for a feed-forward compensation since it does not rely on the time-consuming identification of a complex hysteresis model combined with an numerically expensive inversion algorithm.

VII. Conclusion

In this paper the problem of sinusoidal magnetization of a ferro-magnetic sample using the inverted hysteresis from an identification is addressed. The main problem is the magnetic hysteresis of the material, which poses a strong non-linearity between the input voltage and the resulting magnetization. A feed-forward approach yields good results to overcome this problem for a wide range of input amplitudes and frequencies.

A Classical Preisach Model in the Everett formulation is used for identification and the Everett map is the basis for the model inversion. The Everett map is measured using First Order Descending (FOD) curves, which are recorded during the initial identification phase of an experiment. After computation of the according input voltage the experiment can be started and the sinusoidal magnetization is achieved with a high level of accuracy even without feed-back control. Alternatively, a heuristic inverse is presented, which allows much faster and easier computation of the input voltage and also yields very good results. Since the proposed method is not based on an explicit hysteresis model the time-consuming measurements for identification of the model can be omitted.

The overall control is done by a laptop-computer using LabVIEW and MATLAB. Only two additional boards for signal conditioning and control are used as interfaces between laptop and experimental setup. The complete user interface is programmed as VIs.

The feed-forward control achieves very good results in guaranteeing a sinusoidal magnetization, and proves to be quite robust with respect to different materials, amplitudes, and frequencies. A new approach of an heuristic inversion for periodic signals is presented, and the performance is compared to the inversion using Everett maps. This method seems to outperform the Everett inversion, however, a high acurracy in the measurement procedure must be guaranteed. The whole problem poses a high demand on hardware equipment, since small offsets and drifts will deteriorate the performance of the inversion regardless of the method.

Future work should cover the development of a feedback controller in order to guarantee stable performance under an even wider range of operating conditions, and possible refinements of the model considering dynamic effects.

References

[1] ASTM. *A 932/A 932M-95 Standard Test Method for Alternating-Current Magnetic Properties of Amorphous Materials at Power Frequencies Using Wattmeter-Ammeter-Voltmeter Method with Sheet Specimen.*

[2] R. Ben Mrad and H. Hu. Dynamic modeling of hysteresis in piezoceramics. *IEEE/ASME International Conference on Advanced Intelligent Mechatronics Proceedings*, pages 510–515, 2001.

[3] Giorgio Bertotti. Dynamic generalization of the scalar Preisach model of hysteresis. *IEEE Transactions on Magnetics*, 28(5):2599–2601, 1992.

[4] Giorgio Bertotti. *Hysteresis in Magnetism.* Academic Press, 1998.

[5] B.D. Coleman and M.L. Hodgdon. On a class of constitutive relations for ferromagnetic hysteresis. *Archive for Rational Mechanics and Analysis*, 99(4):375–396, 1987.

[6] Edward Della Torre. Hysteresis modeling. *COMPEL*, 17(6):682–689, 1998.

[7] Edward Della Torre. *Magnetic Hysteresis.* IEEE Press, 1999.

[8] T. Doong and I.D. Mayergoyz. On numerical implementation of hysteresis models. *IEEE Transactions on Magnetics*, 21(5):1853–1855, 1985.

[9] János Füzi. Computationally efficient rate dependent hysteresis model. *COMPEL*, 18(3):445–457, 1999.

[10] Olaf Henze and Wolfgang M. Rucker. Identification procedures of Preisach model. *IEEE Transactions on Magnetics*, 38(2):833–836, 2002.

[11] Marion L. Hodgdon. Applications of a theory of ferromagnetic hysteresis. *IEEE Transactions on Magnetics*, 24(1):218–221, 1988.

[12] Marion L. Hodgdon. Mathematical theory and calculations of magnetic hysteresis curves. *IEEE Transactions on Magnetics*, 24(6):3120–3122, 1988.

[13] Jia-Tzer Hsu and Khai D.T. Ngo. A Hammerstein-based dynamic model for hysteresis phenomenon. *IEEE Transactions on Power Electronics*, 12(3):406–413, 1997.

[14] H. Hu and R. Ben Mrad. On the classical Preisach model for hysteresis in piezoceramic actuators. *Mechatronics*, 13:85–94, 2003.

[15] Declan Hughes and John T. Wen. Preisach modeling of piezoceramic and shape alloy hysteresis. *Smart Materials and Structures*, 6:287–300, 1997.

[16] Gary W. Johnson and Richard Jennings. *LabVIEW Graphical Programming*. McGraw-Hill, 2001.

[17] F. Liorzou, B. Phelps, and D.L. Atherton. Macroscopic models of magnetization. *IEEE Transactions on Magnetics*, 36:418–428, 2000.

[18] I.D. Mayergoyz. Dynamic Preisach models of hysteresis. *IEEE Transactions on Magnetics*, 24(6):2925–2927, 1988.

[19] Samir Mittal and Chia-Hsiang Menq. Hysteresis compensation in electromagnetic actuator through preisach model inversion. *IEEE/ASME Transactions on Mechatronics*, 5(4):394–409, 2000.

[20] Jürgen Schäfer and Hartmut Janocha. Compensation of hysteresis in solid-state actuators. *Sensors and Actuators*, 49:97–102, 1995.

Authors

Martin Kozek is with the Vienna University of Technology, A-1040 Vienna, Austria (email: kozek@impa.tuwien.ac.at).

Bernhard Gross is with the Vienna University of Technology, A-1040 Vienna, Austria (email: kozek@impa.tuwien.ac.at).

Manuscript received June 20, 2005. This work was supported in part by the company VOEST-ALPINE Mechatronics GmbH, A-4031 Linz, Austria.